

NOTE

About the Random Walk from Many Injection Points

L. Zaninetti

Dipartimento di Fisica Generale, Via Pietro Giuria 1, 10125 Torino, Italy

E-mail: zaninetti@to.infn.it

Received June 11, 1998; revised May 24, 1999

Key Words: models; numerical methods; diffusion processes.

1. INTRODUCTION

The random walk on a discrete lattice has been analysed in completely different fields such as chemistry [1, 2], ecology [3, 4], and general physics [5, 6]. The general idea has been to insert a diffusion point at the centre of a 1D, 2D, or 3D discrete lattice and to follow the evolution from an analytical or numerical [7–9] point of view. Here we will start by analysing the stationary state of the random walk in 2D (Section 2) with only one diffusion point at the centre of the lattice. Once the structural behaviour of the visitation grid, as predicted in [8, 9], has been confirmed (in particular the existence of 3 different zones), we continue by inserting the diffusion on a 2D and 3D lattice (Section 3) from many injection points. Finally in Section 4, two applications of the developed theory concerning the field of the astrophysics are reported.

2. THE 2D RANDOM WALK

The random walk in the plane is begun by adopting the following rules:

1. The process starts in the middle of the grid of dimension $NDIM$.
2. The random walk is then performed with equal steps (one lattice point) having four possible directions (up, right, down, and left).
3. Every time a grid point is reached, the two-dimensional array that memorises the times a grid point has been visited is increased by one.

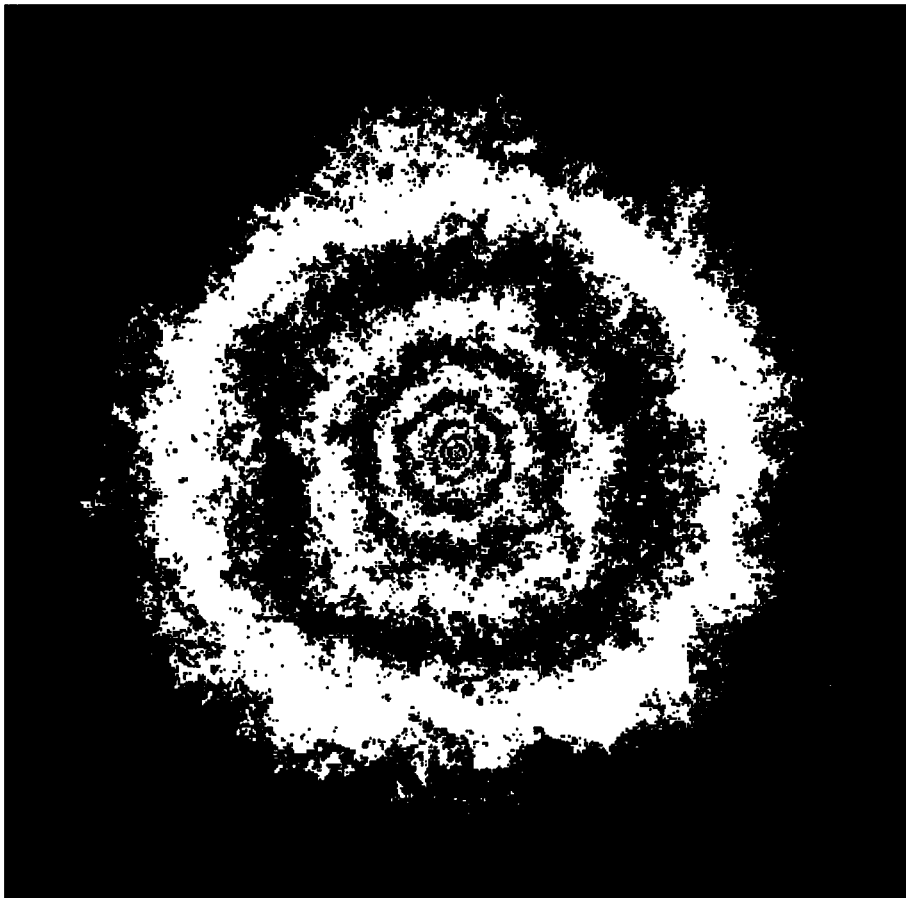


FIG. 1. Contours representing the number of distinct sites visited by NPOINTS walkers. NDIM = 500, SIDE = 100, NPOINTS = 1000.

4. When the boundaries of circular shape are reached the process restarts from point 1.
5. The process stops after NPOINTS trials.

Once the random walk is terminated, the ISO-contours of the two-dimensional array representing the visitation points are made by using two different methods:

1. Traditional contouring to display a surface function of two variables.
2. Using different colours (black and white) to mark every pixel. This technique, developed to represent the Mandelbrot set, avoids the smoothing of the canonical contours.

Here a pseudo-colour algorithm is used and Fig. 1 clearly shows the increase of the roughness with distance from the centre. The properties of the number of distinct sites visited when there are N random walkers are analysed in [1] from an analytical point of view. Here we are interested in the stationary state ($t \rightarrow \infty$) and we assume in analogy with [1] that the visitation number $\mathcal{N}_v(x) \approx P_{surv}(x) \approx ae^{-bx}$ where x is the distance (or the number of pixels) from the diffusion centre and P_{surv} is the probability of surviving at a distance x . On applying

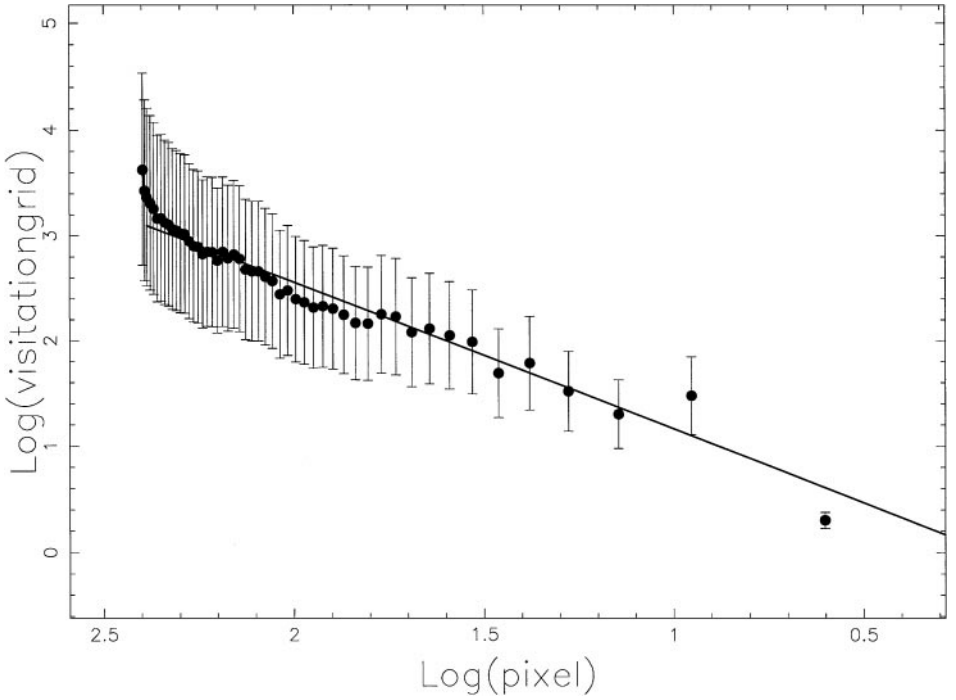


FIG. 2. Cut of the matrix representing the visitation grid: NDIM = 500, SIDE = 100, NPOINTS = 1000, $b(\text{first phase}) = 23.74$, and $b(\text{second phase}) = 1.393$.

the logarithm, the following will easily be found,

$$\text{Log}(\mathcal{N}_v) \approx \text{Log } a - bx \quad (1)$$

and we can therefore search for a linear behaviour in the Log(distance) versus Log(visitation grid). In effect two distinct zones, I and II, are easily found plus an increase of the undulation in phase II; see Fig. 2.

At this point, the algorithm is generalised by introducing the concept of multiple injection points (in the following IP). In the previous case, there was only one injection point of the particles which was exactly in the middle of the grid, and now many IP can be taken into account. In order to continue, the boundary conditions should now be better specified so as to introduce equal area of walk relative to the different IP. Therefore, the concept of a forbidden area is introduced using the following algorithm:

1. First, an area side \times side is chosen; the IP are then generated by a random process with coordinates $x \in R_1$ in $[x_l, x_u]$ and $y \in R_2$ in $[y_l, y_u]$; here $x_l = y_l = red2d \times side$ and $x_u = y_u = side - red2d \times side$. Here $red2d$ is the reduction factor in 2D.
2. The minimum distance, r_{min} , between the IP and the four sides of the box is extracted.
3. The distance from the nearest IP, r_{near} , is computed for every grid point. If $r_{near} > r_{min}$, this grid point is forbidden to the random walk.
4. The random walk is started with a certain number of IP, each one experiencing NPOINTS random walkers. Every time a forbidden zone is reached we start with another particle.

This algorithm is now tentatively described through the following lines of pseudo-code:

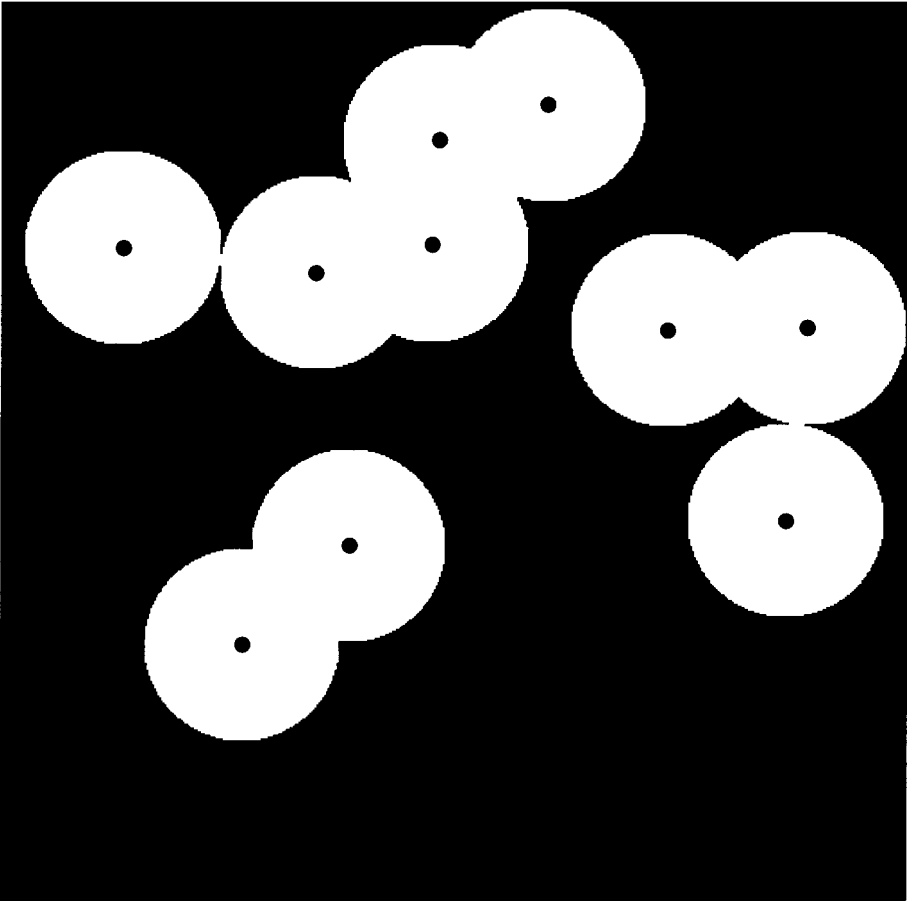


FIG. 3. The forbidden zone marked in black, the IP with circles.

```

do i=1 to IP
  find NPOINTS of the considered IP
  do j=1 to NPOINTS
    make the random walk
    if we reach the forbidden zone then
      stop the cycle
    end if
  end do
end do
end do

```

A typical run of the forbidden zone is represented in Fig. 3 and the resulting contours of ISO-visited zones in Fig. 4 using a colour algorithm.

3. THE 3D RANDOM WALK

We can now consider the extension to the third dimension which requires a few different points:

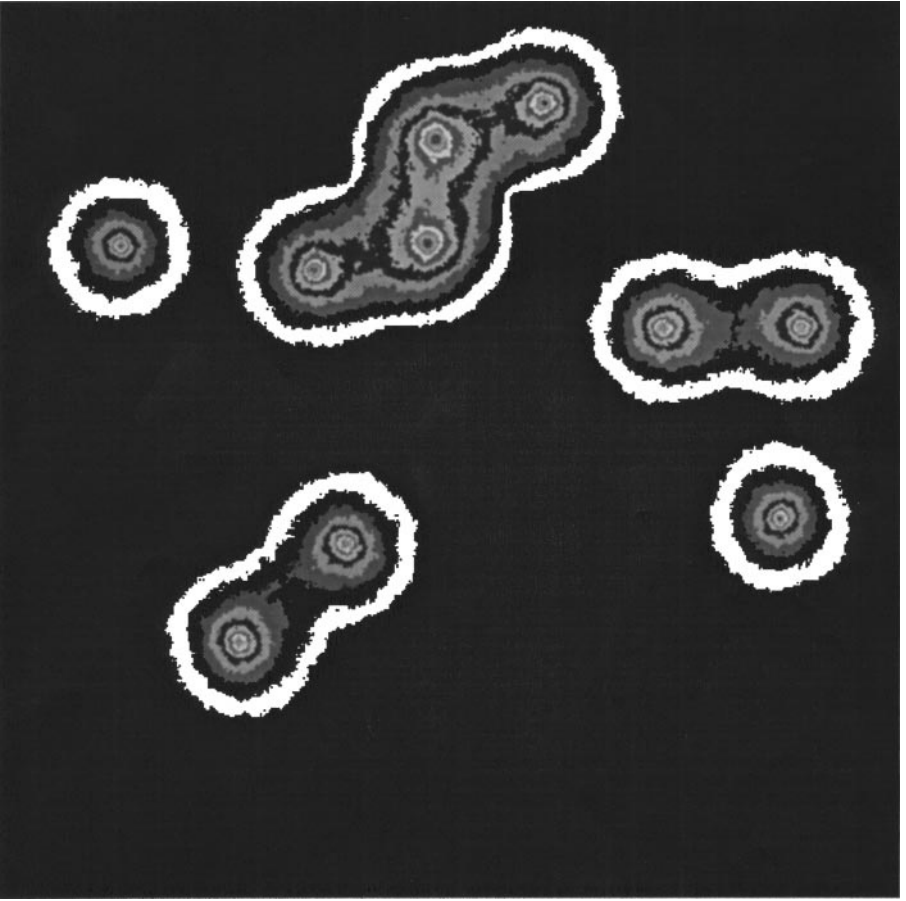


FIG. 4. Colour contours representing the number of distinct sites visited by $NPOINTS \times IP$ walkers. $IP = 10$, $NPOINTS = 2000$, $NDIM = 500$, $SIDE = 100$, $RED2D = 0.05$.

- The random walk has now six degrees of freedom.
- The forbidden area now becomes a volume. Attention should be given to the displacement of the IP in the box and the following procedure is suggested:

1. The volume that the IP are occupying is computed: the minimum distance of the IP from a side is now zero.

2. This volume of factor *red* is then reduced and the IP are reinserted into the box in an encapsulated fashion. Now the minimum distance r_{min} from a face is increased.

3. For every lattice the distance is computed from the nearest IP, r_{near} . If $r_{near} > r_{min}$, this point is forbidden to the random walk.

- The number of visits is memorised on a three-dimensional grid $T(i, j, k)$.

In order to examine a practical example, IP1 IP were inserted in a first torus and IP2 IP in a second TORUS. Geometrically speaking, the two tori are joined like two links of a chain. These IP are reported in Fig. 5 and in order to take into account the great variety of perspectives, the observers parameters are introduced, which are the two angles of viewpoint from the centre of the work-box in degree ϕ (angle in the X-Y plane) and θ (vertical angle from the X-Y plane).

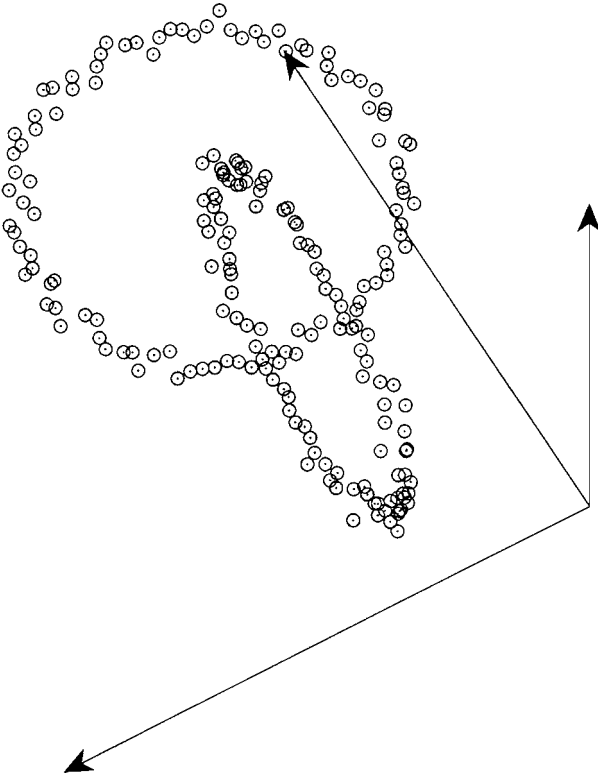


FIG. 5. The 3D display of the IP: $\theta = 30$ and $\phi = 30$.

A problem now arises concerning the visualisation of the three-dimensional grid $A(i, j, k)$. A first visualisation process consists in producing the contours of a slice of the 3D grid: in other words an index is fixed over three (for example, the one in the middle of z) and the resulting 2D grid is transmitted to the contouring routines; see, for example, Fig. 6.

The adopted notation in the text and figures of this section is

NDIM	number of rows /columns eventual depth of the lattice
NPOINTS	number of trials each one with different initial seed
IP	sites of injection of the random walk
r_{min}	minimum distance between the IP and the sides/faces of the box
r_{near}	distance of the pixel from the nearest IP
red	reduction of the initial volume
IP1, IP2	number of IP of the first and second torus
$coef$	parameter that fixes the isovalue of the 3D array t
$side$	physical dimension of the box
NCONT	parameter that fixes the number of contour levels.

4. EXAMPLES

The theory already developed could be applied to experimental physics [10] or to astrophysics. In the following subsection, two applications will be shown of diffusion on a 3D

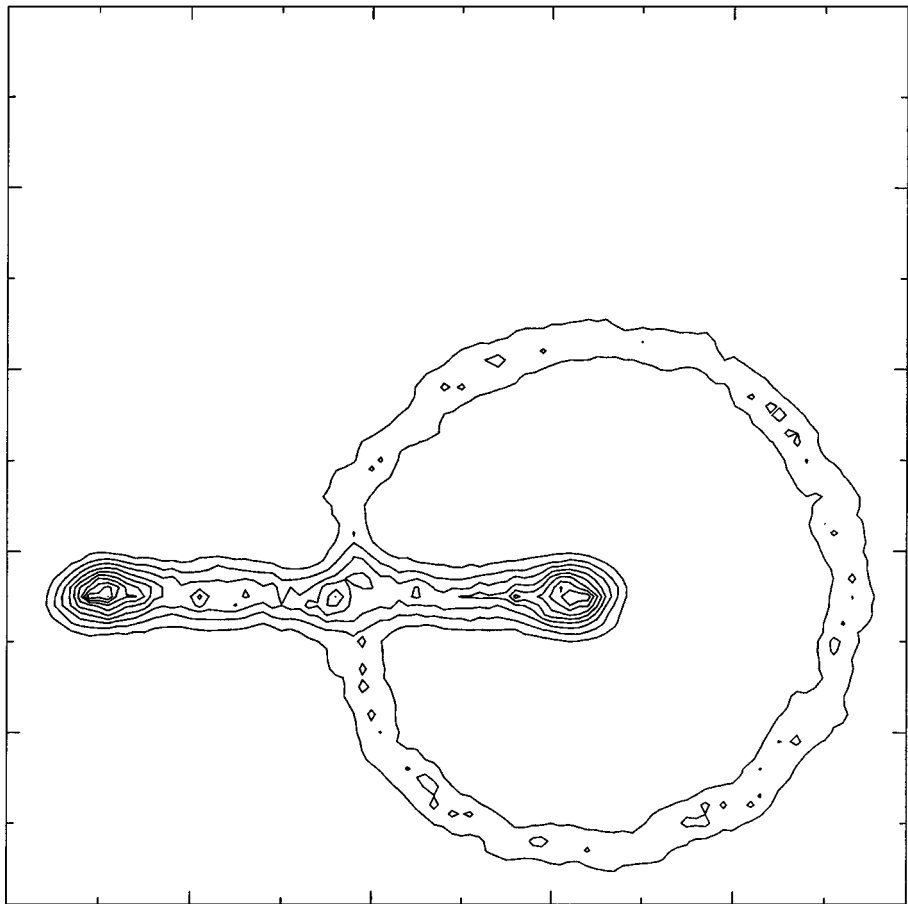


FIG. 6. Contours of a slice of the visitation grid: IP1 = 100, IP2 = 100, IP = 200, NPOINTS = 100, NDIM = 100, NCONT = 10, and red = 0.7.

lattice belonging to astrophysics. Another way to visualise the 3D visitation grid is to sum the elements along the line of sight. From a practical point of view the final result will be a two-dimensional matrix $A_{i,j}$ representing the visitation grid

$$A_{i,j} = \sum_{k=1}^{NDIM} T_{i,j,k}. \quad (2)$$

The astrophysical counterpart of such a operation is the so-called “thin layer approximation.”

4.1. SN

Supernova explosions produce an expanding shell which interacts with the ISM. In the layer of interaction between the expanding shell and the ISM, there is a production of knotty structures due to the development of the Rayleigh–Taylor instabilities. In this case, we place our IP between two radius R_{max} and R_{min} representing the expansion layer of the SN. The number of IP are fixed and in order to be more realistic, a fractal distribution of the number of trials is provided,

$$f(N) = C \frac{1}{N^D}, \quad (3)$$

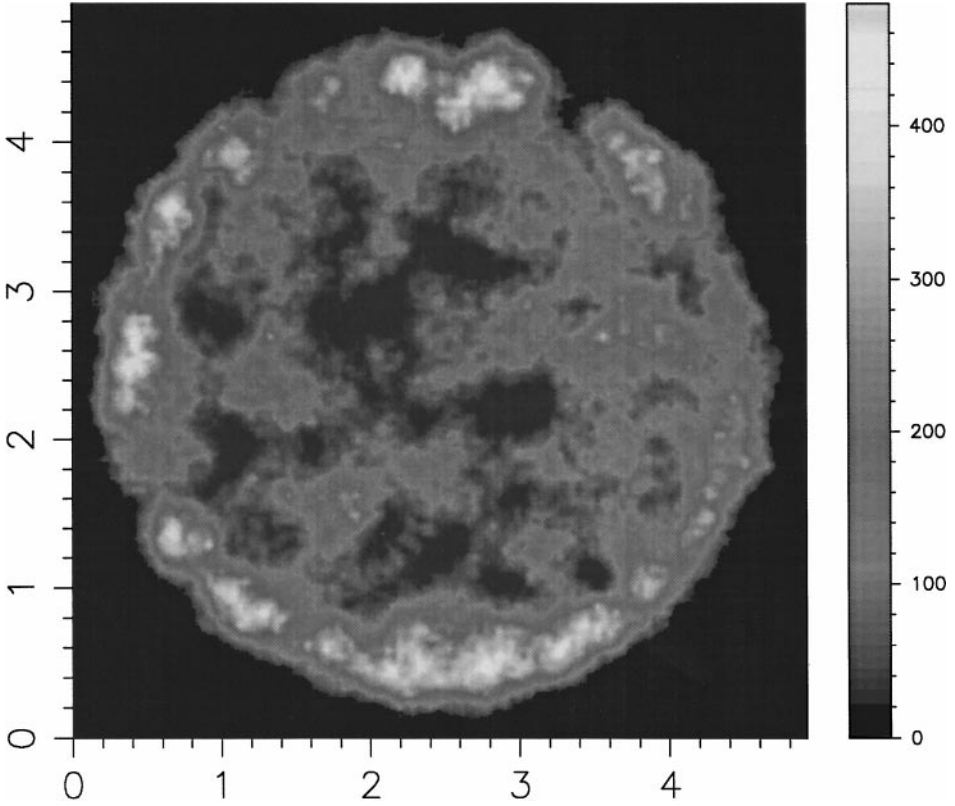


FIG. 7. Colour contours of the two-dimensional surface representing the emissivity in a thin layer with IP points and fractal distribution of the number of trials in 3D. The physical parameters are $IP = 900$, $NDIM = 120$, $red = 0.7$, $N_{max} = 30$, $N_{min} = 10$, $R_{max} = 2.5$ pc, $R_{min} = 0.22$ pc, and $SIDE = 5$ pc.

where the C take the value

$$C = \frac{1 - D}{N_{max}^{-D+1} - N_{min}^{-D+1}}, \quad (4)$$

where N_{min} and N_{max} are the minimum and maximum number of trials possible in each IP. The diameter of the known remnants spans the range from 3 to 60 pc and attention is fixed on Cas A and its possible diameter of 5 pc [11]. Some typical observational features such as edge brightening and presence of knotty structures are reproduced in the simulation of Fig. 7.

Adopted notation in the text and figures of this section is

R_{max}, R_{min}	maximum and minimum radius of the shell of emission
N_{min}, N_{max}	minimum and maximum number of trials for each IP
C	constant in front of the fractal distribution.

4.2. H-H Objects

We know that sometimes an optical jet can be observed connected with molecular outflows in young stellar objects. Often they consist of a chain of knots observed, for example, in the light of S_{II} . The shape of these jets could be simulated through the theory of the

Kelvin–Helmholtz instabilities with the addition of artificial noise. All the details are explained in [12]. The building blocks of this theory will now be briefly reviewed. We start from observable quantities that can be measured on the radio-maps such as the total length L_{obs} , the wavelength λ_{obs}^1 of the wiggles along the jet, the distance λ_{obs}^0 between the knots, and the final offset ΔL_{obs} of the centre of the jet.

These observable quantities are identified with the following theoretical variables,

$$\lambda_{max}^1 = \lambda_{obs}^1, \quad (5)$$

$$\lambda_{max}^0 = \lambda_{obs}^0, \quad (6)$$

$$A_0 \exp\left(\frac{L}{Mt_{ad}a}\right) = \Delta L_{obs}, \quad (7)$$

$$nl_e = L_{obs}, \quad (8)$$

where $t_{ad} = t_{min} \cdot s_i / a$.

We then have a theoretical expression for t_{min} the minimum time scale of the instability, λ_{max} the wavelength connected with the most unstable mode, and l_e the distance over which the most unstable mode grows by a factor e. The physical parameters that allow these theoretical parameters to be expressed are M and v_0 once m is fixed. These parameters could then be found through the set of nonlinear equations previously reported. More realistic simulations are then obtained by introducing *noise*; the blobs will be placed at a position given by a pseudo-random real number taken from a normal (Gaussian) distribution with mean \bar{x} , where \bar{x} is the predicted distance, and standard deviation σ where $\sigma = \lambda_1 / noise$. The circles of the two-dimensional blobs are then simply transformed into spheres. The number of IP is proportional to the jet averaged radius and the number of trials is equal for every IP. Choosing one object, for example, HH34 [13], the following observational parameters are measured on the optical image:

$$L_{obs} = 48 \text{ averaged radius units}$$

$$\lambda_{obs}^0 = 4.0 \text{ averaged radius units}$$

$$\lambda_{obs}^1 = 19.2 \text{ averaged radius units}$$

$$\Delta L_{obs} = 0.96 \text{ averaged radius units}$$

$$\alpha = 15 \text{ degree}$$

$$scaling = 1.1$$

$$noise = 0.8.$$

The four nonlinear equations are then solved and the following numerical values are found:

$$n = 2.75$$

$$M = 17.28$$

$$v_0 = 9.61$$

$$A_0 = 5.57 \cdot 10^{-3}.$$

The final result of the simulation is reported in Fig. 8.

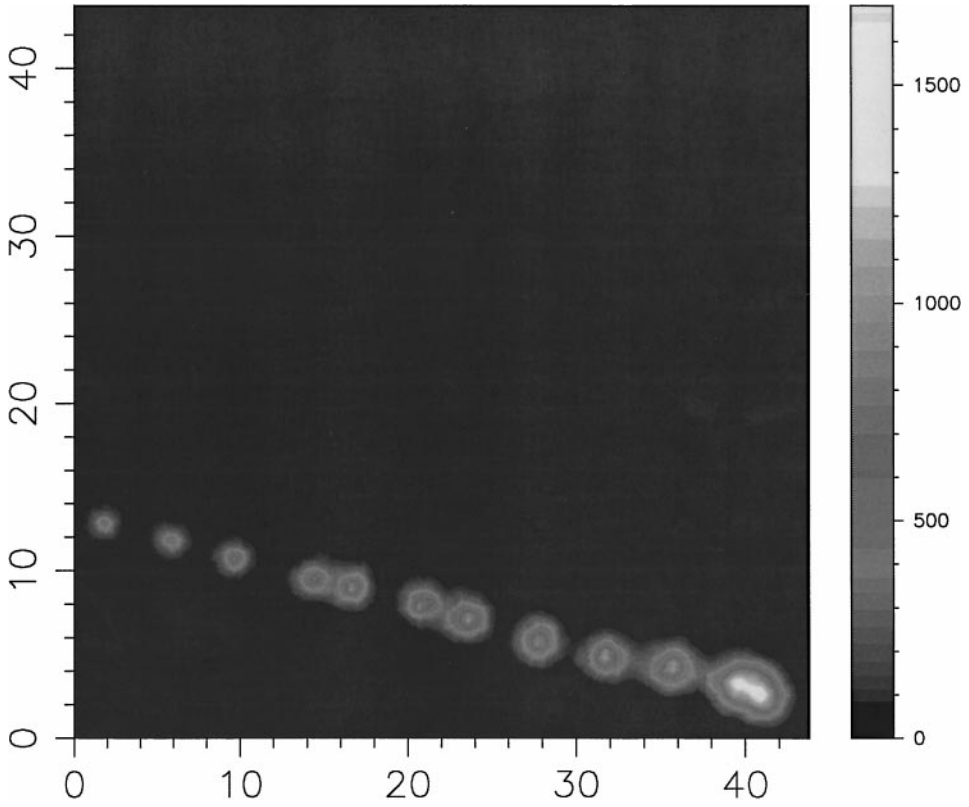


FIG. 8. Colour contours of the two-dimensional surface representing the optical shocked emission of HH-34. The physical parameters are $IP = 643$, $NPOINTS = 10$, $NDIM = 120$, and $red = 0.8$. The coordinates are expressed in averaged jet-radius units.

Adopted notation in the text and figures in this section on H-H objects is

m	azimuthal number
n	number of e-folding lengths
M	Mach number considered
v_0	ratio of the density inside to that outside
L_{obs}	length of the jet in averaged radius-units
ΔL_{obs}	lateral displacement in averaged radius-units
A_0	amplitude of the oscillations
t_{min}	time scale of the more unstable mode
λ_{max}	wavelength of the more unstable mode
l_e	length over which the most unstable mode grows of by a factor e
<i>scaling</i>	x-displacement over jet's length on the map
α	angle of rotation from the horizontal position
<i>noise</i>	deviation from the predicted distance.

5. CONCLUDING REMARKS

The random walk on a 2D or 3D discrete lattice could be set up once the concept of forbidden zone is introduced so as to maintain the symmetry in the process of diffusion. In

order to visualise such phenomena, the traditional colour code algorithm has been used in two dimensions and the ISO-density contours in three dimensions. The developed technique is useful in giving a theoretical framework to the diffusion images of astrophysical objects: here, the SN remnants and optical jets were analysed.

ACKNOWLEDGMENT

The numerical code uses the subroutines extracted from “NUMERICAL RECIPES” for mathematical help and PGPLOT 5.2 as the plotting package.

REFERENCES

1. R. Czech, *J.Chem. Phys.* **91**, 2498 (1989).
2. P. Bordewijk, *Chem. Phys. Lett.* **32**, 592 (1975).
3. J. G. Skellam, *Biometrika* **38**, 196 (1951).
4. L. Edelstein-Keshet, *Mathematical Models in Biology* (Random House, New York, 1988).
5. C. A. Condat, *Phys. Rev. A* **41**, 3365 (1990).
6. G. H. Vineyard, *J. Math. Phys.* **4**, 1191 (1963).
7. M. F. Shlesinger, *Nature* **355**, 396 (1992).
8. H. Larralde, P. A. Trunfio, S. Havlin, H. E. Stanley, and G. H. Weiss, *Nature* **355**, 423 (1992).
9. H. Larralde, P. A. Trunfio, S. Havlin, H. E. Stanley, and G. H. Weiss, *Phys. Rev. A* **45**, 7128 (1992).
10. H. Larralde, Y. Lereah, P. A. Trunfio, J. Dror, S. Havlin, R. Rosenbaum, and H. E. Stanley, *Phys. Rev. Lett.* **70**, 1461 (1993).
11. D. A. Green, *MNRAS* **209**, 449 (1984).
12. L. Zaninetti, *A&A* **223**, 369 (1989).
13. R. Mundt, *Circumstellar Matter*, edited by Appenzeller and Jordan (Reidel, Dordrecht, 1987), p. 147.